Diversity of glucocorticoid receptor signaling: molecular mechanisms and therapeutic implications

Viho, E.M.G.

7

The hippocampal response to acute corticosterone elevation is altered in a mouse model for Angelman syndrome

EVA M. G. VIHO*, A. MATTIJS PUNT*, BEN DISTEL, RENÉ HOUTMAN, JAN KROON, YPE ELGERSMA, ONNO C. MEIJER

*both authors contributed equally

Int J Mol Sci. 2022, Dec 24; 24(1):303

ABSTRACT

Angelman Syndrome (AS) is a severe neurodevelopmental disorder, caused by the neuronal absence of the ubiquitin protein ligase E3A (UBE3A). UBE3A promotes ubiquitin-mediated protein degradation and functions as a transcriptional coregulator of nuclear hormone receptors, including the glucocorticoid receptor (GR). Previous studies showed anxiety-like behavior and hippocampal-dependent memory disturbances in AS mouse models. Hippocampal GR is an important regulator of the stress response and memory formation, and we therefore investigated whether the absence of UBE3A in AS mice disrupted GR signaling in the hippocampus. We first established a strong cortisol-dependent interaction between the GR ligand binding domain and a UBE3A nuclear receptor box in a high-throughput interaction screen. *In vivo*, we found that UBE3A-deficient AS mice displayed significantly more variation in circulating corticosterone levels throughout the day compared to wildtypes (WT), with low to undetectable levels of corticosterone at the trough of the circadian cycle. Additionally, we observed an enhanced transcriptomic response in the AS hippocampus following acute corticosterone treatment. Surprisingly, chronic corticosterone treatment showed less contrast between AS and WT mice in the hippocampus and liver transcriptomic responses. This suggests that UBE3A limits the acute stimulation of GR signaling, likely as a member of the GR transcriptional complex. Altogether, these data indicate that AS mice are more sensitive to acute glucocorticoid exposure in the brain compared to WT mice. This suggests that stress responsiveness is altered in AS which could lead to anxiety symptoms.

key words: Stress, Angelman syndrome, Glucocorticoid receptor, Ubiquitin-protein ligase E3A, Hippocampus.

INTRODUCTION

Angelman Syndrome (AS) is a neurodevelopmental disorder characterized by severe intellectual disability, motor deficits, anxiety, speech impairments, ataxia, sleep disturbances, and epilepsy [1–3]. AS is caused by the deficiency or loss-of-function of the ubiquitin protein ligase E3A (UBE3A) in neurons [4, 5]. The *UBE3A* gene is located on chromosome 15 in a region (15q11.2-13.1) that is subjected to neuron– and paternal–specific genomic imprinting, making the maternal allele of *UBE3A* the sole source of UBE3A protein in mature neurons. Chromosomal aberrations such as deletions, uniparental disomy, imprinting defects, or point mutations that affect the integrity of the maternal *UBE3A* gene lead to the complete loss of neuronal UBE3A, resulting in AS [6–10]. UBE3A is an E3-ligase involved in the ubiquitin-proteasome cascade, a system required for the breakdown and recycling of redundant or defective proteins [11–14]. Mutations affecting UBE3A activity or its nuclear localization lead to AS, suggesting that UBE3A plays an important role in the nucleus [15–18]. Notably, UBE3A contains short leucine-rich (LxxLL) binding motifs, also known as nuclear receptor boxes (NR-boxes) and has been reported to be a transcriptional coregulator of nuclear hormone receptors, likely independent of its ligase function [19–22]. Since loss of UBE3A ligase activity leads to AS [15, 16], the exact contribution of UBE3A as a ligase-independent transcriptional coregulator in the context of AS pathophysiology remains understudied. The GR is a ligand-dependent transcription factor that plays a critical role in stress response and subsequent adaptation [23–26]. The GR is activated by glucocorticoid hormones, such as cortisol which is predominant in humans and corticosterone which is exclusive in mice. Glucocorticoid release into the circulation is controlled by the hypothalamic pituitary adrenal (HPA) axis [27] and follows a circadian rhythm with high hormone levels at the beginning of the active phase and lower levels during the resting phase [28, 29]. Upon activation, the GR changes conformation resulting in its nuclear translocation. In the nucleus, the GR interacts with other transcription factors or directly binds to palindromic DNA sequences called glucocorticoid-response elements (GRE) and recruits coregulator proteins to regulate gene expression [30]. The availability and recruitment of GR coregulators is highly context-specific, which leads to a large diversity in GR-driven transcriptomes throughout the brain and between cell types within one brain region including the hippocampus [31, 32]. Disrupted GR signaling in the hippocampus of UBE3A-deficient AS mice has been associated with learning disabilities and anxiety-like behavior [33]. Furthermore, UBE3A-deficient AS mice are known to be hypersensitive to diet-induced liver steatosis [34], and previously showed metabolic disturbances resulting from an altered circadian rhythm [35]; characteristics that have been related to disruptions in GR signaling [36–38]. However, the molecular

mechanisms underlying the UBE3A modulation of GR signaling are not fully understood. Here, we aimed to better understand the interaction between UBE3A and GR, including the transcriptomic effects of acute or chronic corticosterone treatment on GR signaling in the hippocampus and liver tissue of WT and UBE3A-deficient AS mice.

MATERIALS AND METHODS

1. Microarray Assay for Realtime Coregulator-Nuclear receptor Interaction (MARCoNI)

The GR is a nuclear receptor with two activation function domains (AF1 and AF2), a DNA-binding domain (DBD) and a ligand binding domain (LBD). GR interactions with coregulator motifs via its LBD were assessed in the presence of 1 μM cortisol compared to vehicle (dimethyl-sulfoxide, DMSO), as previously described [39]. A total of 154 short leucine rich (LxxLL) binding motifs representing 64 known nuclear receptor coregulators were attached to the solid phase of the PamChip® array. The GR LBD tagged with Glutathione S-transferase (GST) was overexpressed in HEK 293T cells. The coregulator-derived motifs were incubated with the HEK 293T cell lysates containing GR LBD-GST, the ligand (DMSO or 1 μM cortisol), and a GST-specific antibody coupled to a fluorophore. The interaction between GR LBD and the coregulator motifs was assessed by detection of the fluorophore immunofluorescent signal. For all coregulator motifs, each treatment condition had four replicates from which the mean and the standard error of the immunofluorescent signal were calculated. The modulation index (MI) of each coregulator motif was calculated as the $\log_{10}$-transformed ratio of the mean signal in the presence of cortisol to the mean signal in the presence of DMSO. The standardized MARCoNI assay numbered the LxxLL domain amino acids based on the sequence of the human isoform 2 of UBE3A, however this isoform is lowly expressed [40]. Therefore, the sequence of isoform 3 of UBE3A, in concordance with the MANE annotation [41], was further used for amino acid numbering in the current study.

2. Cell culture

2.1. GR activity

Wildtype (WT) and *UBE3A* knock-out (*UBE3A*^{KO}) HEK 293T cells [17] were seeded 80,000 cells/well in 24-well plates in culture medium DMEM (1X) + GlutaMAX™ supplemented with 10% Charcoal-stripped fetal bovine serum (FBS), penicillin and streptomycin. The cells were transfected after 24 hours using the FuGENE®HD Transfection Reagent (E2311, Promega Corporation, Madison, U.S.A.) according to

the manufacturer's instructions. Per well, 10 ng human GR plasmid, 25 ng tyrosine aminotransferase GR response element coupled to the firefly-luciferase (TAT1 - GR-dependent reporter gene) [42], 1 ng CMV-renilla (control reporter gene) and 264 ng pcDNA were transfected. One day later, the cells were treated with 0.1% DMSO as vehicle or 0.1 – 1000 nM cortisol. After 24 hours, the medium was removed, the cells were washed once with phosphate-buffered saline (PBS) and lysed to measure GR-dependent luciferase activity using the Dual-Luciferase® Reporter Assay (E1910, Promega Corporation, Madison, U.S.A.). The luminescent signal was measured with SpectraMax®iD3, using SoftMax Pro 7.0.2. Each treatment condition had four replicates and the experiment was performed twice. All data are expressed as the ratio between the reporter gene and the control reporter gene luminescent signal.

2.2. GR stability

UBE3A^{KO} HEK 293T cells were seeded at a density of 150,000 cells/well in 12-well plates and cultured in DMEM (1X) + GlutaMAX™ supplemented with 10% fetal calf serum (FCS), penicillin, and streptomycin. After 24 hours, the cells were transfected with plasmids containing the human GR (750 ng) in combination with different human UBE3A isoform–1 variants (UBE3A^{WT}, UBE3A^{LD}, UBE3A$^{\Delta AZUL}$) (750 ng) using polyethylenimine (PEI) in a ratio DNA:PEI of 1:3. After 48 hours, the cells were treated for eight hours with either vehicle (DMSO) or 1 µM cortisol, alone or in combination with 10 µM MG132 (proteasome inhibitor) or 70 µg/ml cycloheximide (CHX – *de novo* protein synthesis inhibitor). Hereafter the cells were harvested and snap-frozen in liquid nitrogen until further analysis. Cell pellets were lysed in lysis buffer (250 mM sucrose, 20 mM HEPES [pH 7.2], 1 mM $MgCl_2$, 10 U/mL Benzonase), supplemented with the c0mplete Protease Inhibitor Cocktail (11836145001, Roche, Basel, Switzerland). Protein concentrations were determined using BCA Protein Assay Kit (23225, Pierce™ Thermo Fisher Scientific Inc., Waltham, U.S.A.) and a total of 10 µg protein per sample was loaded and run on a 26-well 4-15% Tris-Glycine gel (5671085, Bio-Rad Laboratories, Hercules, U.S.A.). The separated proteins were transferred to a 0.2 mm nitrocellulose membrane (170-4159, Bio-Rad Laboratories, Hercules, U.S.A.) and blocked in TBST (10 mM Tris-HCl [pH 8.0], 150 mM NaCl, 0.1% Tween-20 (P1379, Sigma-Aldrich, St. Louis, U.S.A.), supplemented with 5% (w/v) skim-milk powder (70166-500G, Sigma-Aldrich, St. Louis, U.S.A.) for 30 minutes at room temperature. Membranes were briefly rinsed with TBST, and incubated with primary antibodies overnight at 4 °C. The day after, the membranes were briefly washed in TBST, before incubation with secondary antibodies for an hour at room temperature. Finally, the membranes were washed three times with TBST and three times with TBS and analyzed by measuring enhanced chemiluminescence

or infrared fluorescence (Li-Cor Biosciences, Lincoln, U.S.A.). The following primary and secondary antibodies were used:

Table 1. List of antibodies used to assess GR stability in *UBE3A*^{KO} HEK 293T cells

Antibody target	Antibody species	Supplier	Product number	Dilution
Primary antibodies				
Anti-GR	Rabbit	Cell Signaling Technology, Danvers, U.S.A.	12041S	1:1,000
Anti-β-Actin	Mouse	Chemicon Sigma-Aldrich, St. Louis, U.S.A.	MAB1501R	1:20,000
Anti-GAPDH	Rabbit	Cell Signaling Technology, Danvers, U.S.A.	2118S	1:1,000
Secondary antibodies				
Anti-mouse	Goat	LI-COR, Lincoln, U.S.A	926-32210	1:15,000
Anti-rabbit	Goat	LI-COR, Lincoln, U.S.A	926-68071	1:15,000

Protein band intensities were measured using ImageStudioLite and normalized against β-Actin or GAPDH protein expression. The experiment was performed four times with three to four replicates per condition. The average of all replicates was calculated in each assessment giving a total N=4 for the entire experiment. GR protein levels were expressed as a normalized percentage from the vehicle-treated control group.

3. Animals

WT C57BL/6J male and female 129sv *Ube3a*$^{m+/p-}$ mice (*Ube3a*^{tm1Alb}; MGI 2181811) [43], were crossed to generate F1 hybrid WT and *Ube3a*$^{m-/p+}$ (AS) offspring. The *Ube3a*^{tm1Alb} strain resulted from the deletion of the exon 5 of *Ube3a*, leading to an out-of-frame mutation and loss of UBE3A protein expression in neurons. Adult 10–18-week-old male mice were used in the experiments. Mice were housed in conventional cages with a 12:12 hour light-dark cycle (7:00 AM lights on and 7:00 PM lights off) and *ad libitum* access to food and water. All animal experiments were conducted at the Erasmus MC in Rotterdam, in accordance with the European Commission Council Directive 2010/63/EU (CCD approval AVD101002016791).

3.1. Acute corticosterone exposure

On day 0 of the experiment, blood was withdrawn from WT (n=12) and AS (n=12) mice via tail vein incision, at 8:00 (AM) and 18:00 (PM), to measure baseline circulating corticosterone. Blood samples were kept on ice and centrifuged at 12,000 rpm for five minutes. The plasma was then collected and stored at -20 °C until further processing. On day 5, animals were injected subcutaneously with 3 mg/kg corticosterone (27840, Sigma-Aldrich, St. Louis, U.S.A.) or vehicle (5% ethanol

in PBS) between 9:00 and 11:00 to mimic a transient increase in corticosterone, as previously described [44–46]. Three hours later, animals were sacrificed by cervical dislocation, trunk blood was collected in an EDTA-coated collection tube and kept on ice and centrifuged at 12,000 rpm for five minutes. The plasma was then collected and stored at -20 °C until further processing. The left frontal cortex and the left hippocampus tissues were isolated, snap-frozen in liquid nitrogen and stored later at -80 °C until further processing.

3.2. Continuous corticosterone exposure

On day 0 of the experiment, WT (n=10) and AS (n=10) mice underwent surgery to subcutaneously implant a corticosterone slow-release pellet (20 mg corticosterone, 80 mg cholesterol) or a vehicle pellet (100 mg cholesterol) to mimic a sub-chronic corticosterone exposure, as previously described [47–49]. On day 6, animals were sacrificed by cervical dislocation, and left frontal cortex, left hippocampus and liver tissues were collected, snap-frozen in liquid nitrogen and stored later at -80 °C until further processing.

4. Corticosterone biochemical analysis

To evaluate corticosterone blood levels, plasma samples were analyzed using the Corticosterone HS High Sensitivity EIA kit (AC-15F1, Immunodiagnosticsystems IDS, East Boldon, U.K.) according to the manufacturer's instructions. To calculate the delta PM-AM at baseline, for each animal, the AM corticosterone levels (ng/ml) were subtracted from the PM corticosterone levels (ng/ml).

5. Protein levels measurements in mouse brain and liver tissue

Frozen frontal cortex and liver tissue were lysed with glass beads in RIPA buffer (89900, Pierce™ Thermo Fisher Scientific Inc., Waltham, U.S.A.) supplemented with protease and phosphatase inhibitors (A32959, Pierce™ Thermo Fisher Scientific Inc., Waltham, U.S.A.) using the homogenizer (Zentrimix 380R, Hettich Benelux B.V, Geldermalsen, Netherlands) at 4°C, with 1,500 rpm for 40 seconds. Protein lysates were transferred in a fresh Eppendorf and protein concentrations were determined using a BCA protein assay kit (23225, Pierce™ Thermo Fisher Scientific Inc., Waltham, U.S.A.). All protein lysates were diluted in RIPA to the final concentration of 0.8 µg/µL. Protein expression was measured using the Simple Western™ WES system (ProteinSimple Bio-Techne, Minneapolis, U.S.A.) with the anti-mouse (DM-002, ProteinSimple Bio-Techne, Minneapolis, U.S.A.) or anti-rabbit (DM-001, ProteinSimple Bio-Techne, Minneapolis, U.S.A.) detection modules according to the procedure provided by the manufacturer. The following primary antibodies were used:

Table 2. List of primary antibodies used to assess GR and UBE3A protein levels in animal tissues

Antibody target	Antibody species	Supplier	Product number	Dilution
Anti-GR	Rabbit	Cell Signaling Technology, Danvers, U.S.A.	12041S	1:20
Anti-UBE3A (for brain tissue)	Mouse	Sigma-Aldrich, St. Louis, U.S.A.	E8655	1:20
Anti-UBE3A (for liver tissue)	Mouse	Santa Cruz Biotechnology, Dallas, U.S.A.	sc-166689	1:20
Anti-αβ-tubulin	Rabbit	Cell Signaling Technology, Danvers, U.S.A.	2148S	1:20

6. RNA sequencing (RNA-seq) analysis of mouse hippocampus and liver tissue

Total RNA was isolated from frozen hippocampus and liver tissue using the NucleoSpin® RNA kit (740955.50, Macherey-Nagel, Düren, Germany) and RNA quality was assessed using the RNA 6000 Nano kit on the Bioanalyzer (Agilent, Santa Clara, U.S.A.). All samples had an appropriate RNA Integrity Number (RIN) over 8 with a 28/18s ratio over 1 and were considered suitable for sequencing. Aliquots of total RNA samples were sent for RNA-seq at BGI Genomics (Tai Po, Hong Kong). Stranded mRNA libraries were constructed, and 100-bp paired end sequencing was performed on the DNBseq platform resulting in over 20 million reads per sample. The BioWDL pipeline was used for reads quality control, alignment, and quantification. Quality control was performed using FastQC and MultiQC. Reads were aligned to mm10 using STAR and gene-read quantification was performed using HTSeq-count (BioWDL v5.0.0, https://biowdl.github.io/RNA-seq/v5.0.0/index.html). Output files were merged into a count matrix as input for differential gene expression analysis. DESeq2 (version 1.30.1) was used for normalization of the data (median of ratio's method) and identification of differentially expressed genes in R v4.0.2. Differential exon usage analysis was performed in the mouse cohort exposed to continuous corticosterone to validate UBE3A deficiency at the mRNA level in the AS model (**Fig. S4**).

For the differential gene expression analysis, we selected all genes which were expressed in a minimum of three replicates with more than 20 normalized counts for at least one of the treatment groups. This resulted in 14,611 differentially expressed genes for the hippocampus after acute corticosterone exposure, 14,949 genes for the hippocampus after continuous corticosterone exposure, and 11,988 genes for the liver after continuous corticosterone exposure. The sources of variation between groups were identified using the principal component analysis (PCA). The

contrasts between groups were analyzed for differential expression in a pair-wise comparison.

7. Pathway enrichment analysis

The subset of genes contributing to the differential response to acute corticosterone in AS mice underwent gene ontology (GO)-term and pathway enrichment analyses using the STRING database v11.5 (https://string-db.org/) [50]. We selected the top 10 GO-terms for molecular function (GO:MF), and the top 10 pathways detected in REACTOME. The extent of the enrichment was measured by the strength which represents the $\log_{10}$-transformed ratio between i) the number of genes in the current study that are annotated with a term/pathway and ii) the number of genes that were expected to be annotated with this term/pathway in a random network of comparable size. The false discovery rate (FDR) describes how statistically significant the enrichment is, the p-values are corrected for multiple testing using the Benjamini-Hochberg approach. Enrichment significance is expressed as the -$\log_{10}$(FDR).

8. Single-cell RNA sequencing in the adult mouse hippocampus

The top 20 downregulated and top 20 upregulated genes associated with the differential response to acute corticosterone in AS mice were selected for single-cell expression analysis in the adult mouse hippocampus, as we previously described [32]. Our published dataset allows the exploration of gene expression in 13 different cell types of the adult mouse hippocampus, including glutamatergic neurons, GABAergic neurons, and non-neuronal cells. The current data was expressed using the dotplot function of Seurat v3.1.5 in R v3.6.1 where the Z-Score (scaled and centered normalized expression) represents the average gene expression within one cell type and the size of the dot indicates the percentage of positive cells.

9. Statistics

In the MARCoNI assay, statistical significance was determined by a t-test in R v.4.0.2. For the assessment of GR activity in WT and *UBE3A*^{KO} HEK-293T cells, statistical significance was calculated using the two-way analysis of variance (ANOVA) in GraphPad Prism 9. The EC50 values for both cell lines were determined using GraphPad Prism 9 non-linear fitting and expressed as mean and standard deviation (±SD). The results of GR stability in *UBE3A*^{KO} HEK-293T cells, mouse plasma corticosterone and tissue protein measurements were corrected for outliers using the Grubb's method, all results were expressed as mean and standard error of the mean (±SEM) and statistical significance was calculated using the two-way ANOVA or the Mann-Whitney test in GraphPad Prism 9. In the RNA-seq analysis, an FDR-

adjusted p-value of 0.05 was used as a cut-off to determine differentially expressed genes.

RESULTS

UBE3A interacts with the GR ligand binding domain

The identification of GR coregulatory interactions is essential in the understanding of GR signaling adaptive and maladaptive outcomes. We evaluated the interaction between the GR LBD with an array of known nuclear receptor coregulator binding motifs in the presence of 1 μM cortisol. The short leucine-rich (LxxLL) binding motifs, also known as nuclear receptor boxes (NR-boxes) of 64 known nuclear receptor coregulators were incubated with the GR LBD that was tagged with Glutathione S-transferase (GST). The binding of GR LBD to a coregulator NR-box was detected with an anti-GST antibody coupled to a fluorophore. The modulation index (MI) represents the normalized immunofluorescent signal in the presence of cortisol (**Fig. 1A**). Out of 154 NR-boxes, 54 showed significant interaction with GR LBD in the presence of 1 μM cortisol, as compared to vehicle (**Fig. 1B**). In this subset, we could identify NR-boxes from nuclear receptor coactivators including the SRC family (NCOA1, NCOA2, NCOA3 and NCOA6), PRGC1, and known corepressors such as LCOR and NRIP1 (**Fig. 1B**). The strongest interaction with GR LBD was observed for one NR-box of UBE3A (**Fig. 1B**). This LxxLL motif of UBE3A localized between amino acid 393 and 415 (MI = 1.89, p = 0.03) of the human isoform 3 (UBE3A hIso3) [40]. Another significant interaction was found between GR LBD and a UBE3A hIso3 LxxLL motif situated between amino acid 646 and 668 (MI = 0.55, p = 0.004). We further investigated the effect of UBE3A on GR activity and stability in cultured cells. Here we found that GR activity in response to cortisol was significantly reduced in *UBE3A*^{KO} HEK 293T cells, suggesting that UBE3A can act as a GR transcriptional coregulator in these cells (**Fig. 1C**). Since GR transcriptional activity was previously linked to its proteasomal degradation, we assessed whether UBE3A enhanced the ubiquitin-dependent degradation of cortisol-bound GR. In contrast with the ligase-dead mutant (UBE3A^{LD}), active nuclear (UBE3A^{WT}) and cytosolic UBE3A (UBE3A^{dAZUL}) modestly — but non-significantly — reduced GR levels, as compared to the empty vector (EMPTY). These modest effects could be rescued by inhibiting the proteasome (**Fig. 1D**). However, GR activation by cortisol did not further destabilize GR in the presence of active UBE3A (**Fig. 1E**). Additionally, we did not observe UBE3A-dependent enhancement of GR turnover following the addition of *de novo* protein synthesis inhibitor CHX (**Fig. 1F**). Taken together, these results indicate that it is unlikely that the GR coregulator function of UBE3A relies on the proteasomal

degradation of cortisol-bound GR, and rather support previous findings suggesting this process is largely independent of UBE3A ligase activity.

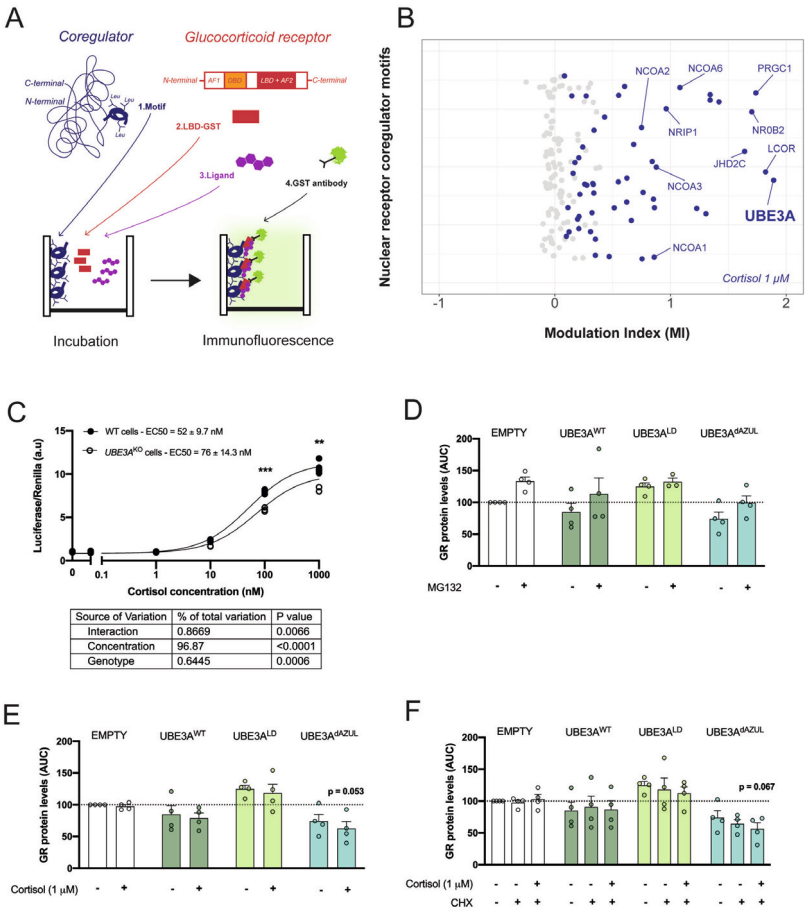

Source of Variation	% of total variation	P value
Interaction	0.8669	0.0066
Concentration	96.87	<0.0001
Genotype	0.6445	0.0006

Figure 1. UBE3A interacts with the GR ligand binding domain and slightly alter GR activity and stability. (A) Schematic representation of the Microarray Assay for Realtime Coregulator-Nuclear receptor Interaction (MARCoNI) applied to the GR. Short leucine-rich binding motifs corresponding to known nuclear receptor coregulators (1. Motif) were incubated with the GR LBD tagged with Glutathione S-transferase (2. LBD-GST) and a GR ligand (3. Ligand). The interaction between a motif and the GR LBD was detected with a GST-specific antibody coupled to a fluorophore (4. GST antibody). **(B)** Interaction of the GR LBD with 154 short leucine-rich binding motifs of 64 known nuclear receptor coregulators as measured by the modulation index (MI) in the presence of 1 µM cortisol. **(C)** GR activity in response to 0.1 nM to 1µM cortisol in WT or *UBE3A* knock-out (*UBE3A*^{KO}) HEK 293T cells as measured in a GR-driven luciferase-reporter assay. **(D)** GR protein levels in *UBE3A*^{KO} HEK 293T cells after transfection of an empty plasmid (EMPTY), wild-type *UBE3A* (UBE3A^{WT}), ligase-dead *UBE3A* mutant (UBE3A^{LD}), or dAZUL *UBE3A* mutant (UBE3A^{dAZUL}) followed by treatment with vehicle (0.01% DMSO) or proteasome inhibitor MG132; **(E)** vehicle or 1 µM cortisol; **(F)** vehicle, *de novo* protein synthesis inhibitor cycloheximide (CHX) or CHX and 1 µM cortisol.

UBE3A deficiency in AS mice alters circulating corticosterone levels

We next evaluated the role of UBE3A in GR signaling *in vivo*. To assess whether UBE3A deficiency in AS mice could interfere with HPA axis activity and alter circadian glucocorticoid release, we measured baseline plasma corticosterone (CORT) levels in UBE3A-deficient AS mice and WT littermates. As expected, WT and AS mice showed significantly higher plasma CORT levels at the beginning of their active phase (PM) as compared to the resting phase (AM) ($p < 0.001$, **Fig. 2A**). Remarkably, AS mice showed low to undetectable levels of CORT at AM, even though at PM the levels were comparable to WT. This makes the daily corticosterone fluctuations in AS mice significantly larger than in WT mice (**Fig. 2B**), which indicates that HPA axis activity is altered in AS mice.

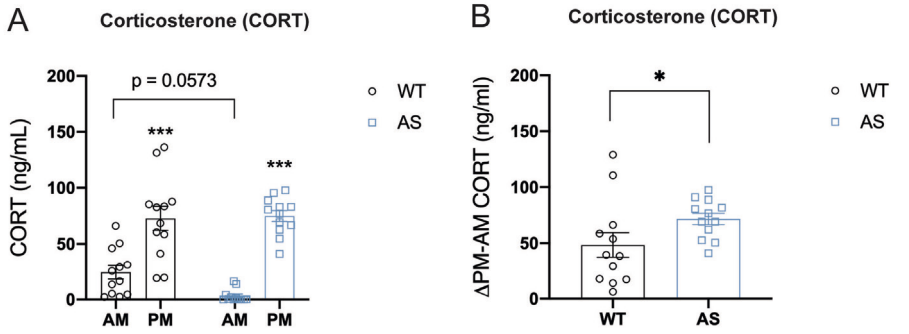

Figure 2. UBE3A deficiency in AS mice alters circulating corticosterone levels. (A) Circulating corticosterone levels in WT and AS mice at the beginning of the resting phase (AM) and the active phase (PM) (ng/mL). **(B)** Difference between PM and AM corticosterone plasma levels in WT and AS mice (ng/mL).

Acute CORT exposure strongly alters hippocampal GR signaling in UBE3A-deficient AS mice

Alterations of HPA axis activity can lead to further disruption of GR signaling in response to abnormal increases in glucocorticoid levels. We compared the hippocampus transcriptomic response in UBE3A deficient adult AS mice and WT littermates in response to acute CORT exposure, using RNA-seq. Hereto, UBE3A-deficient AS mice and WT mice were subcutaneously injected with 3 mg/kg CORT or vehicle, three hours prior to brain tissue collection (**Fig. 3A**). We confirmed the lack of UBE3A protein expression in brain tissue of AS mice ($p < 0.001$) and found that UBE3A levels were not influenced by acute CORT treatment (**Fig. 3B, Fig. S1A**). The PCA analysis on the RNA-seq data revealed that 36% of the variation (PC1 + PC3) was explained by the genotype (AS vs. WT) and treatment (CORT vs. vehicle) effects. The transcriptomic profiles of WT and AS mice largely overlapped upon vehicle

treatment but diverged after CORT treatment (**Fig. 3C**). PC2 corresponded to 18% of the variation and was mostly explained by a single WT mouse, treated with CORT (i.e., sample H8; **Fig. S1B**). This mouse did not display abnormal plasma CORT levels at endpoint (**Fig. S1C**), hence this sample was included in the subsequent analysis.

Upon acute CORT treatment (FDR-adjusted p-value < 0.05), the expression of 283 genes was altered in the hippocampus of WT mice (**Fig. 3D**), as compared to 2,910 genes in AS mice (**Fig. 3E**). Among these genes differentially regulated by CORT, 204 overlapped between WT and AS, 79 were WT-specific, and 2,706 were AS-specific **(Fig. 3D-E**). These results can partially be explained by the slightly elevated GR levels measured in AS brain tissue (p = 0.0594, **Fig 3F, Fig. S1A**), but the magnitude of the transcriptomic effects suggests that UBE3A exerts a limiting effect on GR transcriptional activity in the mouse hippocampus.

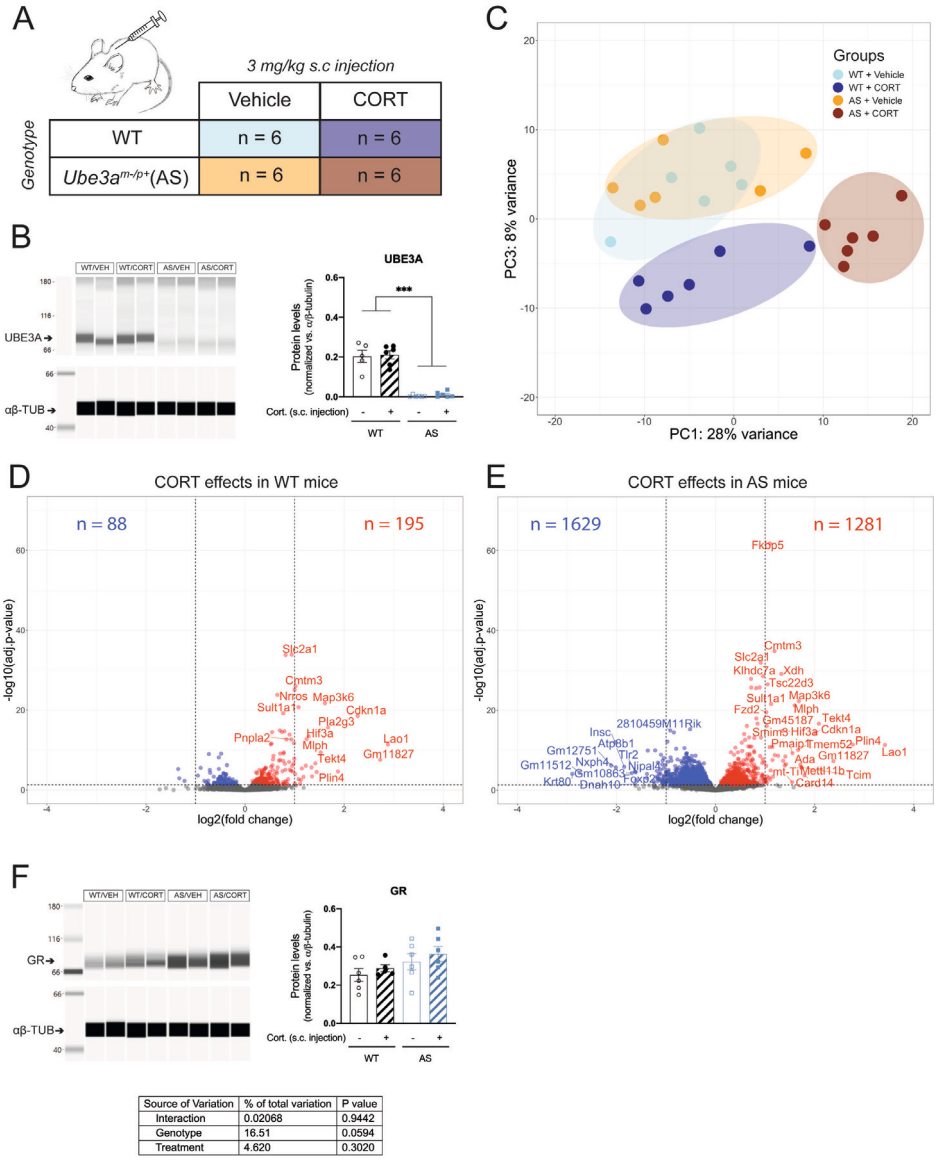

Source of Variation	% of total variation	P value
Interaction	0.02068	0.9442
Genotype	16.51	0.0594
Treatment	4.620	0.3020

Figure 3. Acute corticosterone exposure strongly alters hippocampal GR signaling in UBE3A-deficient AS mice. (A) WT and AS mice were subcutaneously (s.c.) injected with vehicle or 3 mg/kg corticosterone (n = 6/group). **(B)** UBE3A protein expression in the frontal cortex of WT and AS mice after acute treatment with vehicle or corticosterone, normalized against αβ-tubulin levels (αβ-TUB). **(C)** Analysis of hippocampus RNA-seq data principal sources of variance (PCA). **(D)** Volcano plot representing the transcriptomic effects of acute corticosterone treatment in WT mouse hippocampus. **(E)** Volcano plot representing the transcriptomic effects of acute corticosterone treatment in AS mouse hippocampus. **(F)** GR protein expression in the frontal cortex of WT and AS mice after acute treatment with vehicle or corticosterone, normalized against αβ-tubulin levels (αβ-TUB).

Acute CORT exposure influences pathways associated with transcription activity and neurotransmitter signaling in the hippocampus of UBE3A-deficient AS mice

When comparing the CORT treated WT group with the CORT treated AS group, we found 3,890 differentially regulated genes (**Fig. S1D**). Of these, 1,208 genes statistically contributed to the interaction between the genotype and the treatment, and therefore underly the differential response to acute CORT in AS mice (**Fig. S1E**). We performed gene ontology and pathway enrichment analyses on that gene subset and the top 10 GO-terms for molecular functions were associated with amino acid transmembrane transport (solute carrier family – SLC) and transcription activity, including nuclear hormone receptor activity (**Fig. 4A**). This last term included 21 genes regulated by CORT in AS mice, including genes involved in the mediator complex (*Med24*, *Med4*), transcription coactivators (*Snw1*, *Tgfb1i1*, *Wbp2*, *Thrap3*), chromatin remodelers (*Smarce1*, *Hmga1b*, *Sirt1*, *Bcas3*), transcription factors (*Tcf7l2*, *Lef1*, *Nr1h2*, *Tcf7l2*), proteins involved in nuclear receptor import (*Ipo13*) or protein stability (*Sumo2*, *Rnf6*). The top 10 enriched pathways according to the REACTOME database were predominantly involved in mRNA splicing, chromatid cohesion (*Pds5b*, *Rad21*, *Esco1*, *Smc3*, *Wapal*, *Stag1*, *Stag2*) and neurotransmitter signaling (*Ppfia2*, *Ppfia3*, *Stx1a*, *Vamp2*, *Lin7c*, *Slc6a11*, *Slc17a7*, *Cplx1*, *Stxbp1*, *Rab3a*, *Syn1*) (**Fig. 4B**). This suggests that the effects of acute CORT exposure in the brains of AS, but not WT mice are broadly involved in transcription regulation and synaptic transmission.

Acute CORT exposure influences genes in the UBE3A-deficient AS mouse hippocampus that are heterogeneously expressed in hippocampal cell types

We selected the top 40 genes from the 1,208 genes which significantly contributed to the genotype-treatment interaction and characterized their cell type-specific expression using our adult mouse hippocampus atlas (**Fig. 4C**). Two genes from the selected subset were undetectable in the hippocampus cell atlas: *Mir5125* which was not captured by 10x scRNA-seq, and *Adnp*. The expression of genes appeared heterogenous throughout different hippocampal cell types, e.g., *Rfx3* and *Rasal2* were highly expressed in the glutamatergic neurons of the dentate gyrus (DG), while *Ccdc43* and *Prpf33a* expression was higher in CA2 glutamatergic neurons, and *Ezr* expression was specific for astrocytes (**Fig. 4C**). It is interesting to note that many genes that were downregulated by CORT in AS mice were predominantly expressed in non-neuronal cells, considering that these cells still express 50% of UBE3A protein. For example, *Sox10* was specifically expressed in oligodendrocytes, while *Fxyd5* and *Lef1* were exclusively expressed in endothelial cells. We observed only few genes that were highly expressed in neuronal cell types, for instance *Atf5* and *Lypla2* (**Fig. 4C**). Altogether, these results suggest that genes affected by acute

CORT exposure in AS are heterogeneously expressed in mouse hippocampal cell types and sub-regions (DG, CA1-ProS, CA2 and CA3). Each of these cell types may respond differently to reductions in UBE3A levels, thereby featuring specific GR-mediated adaptations to CORT exposure.

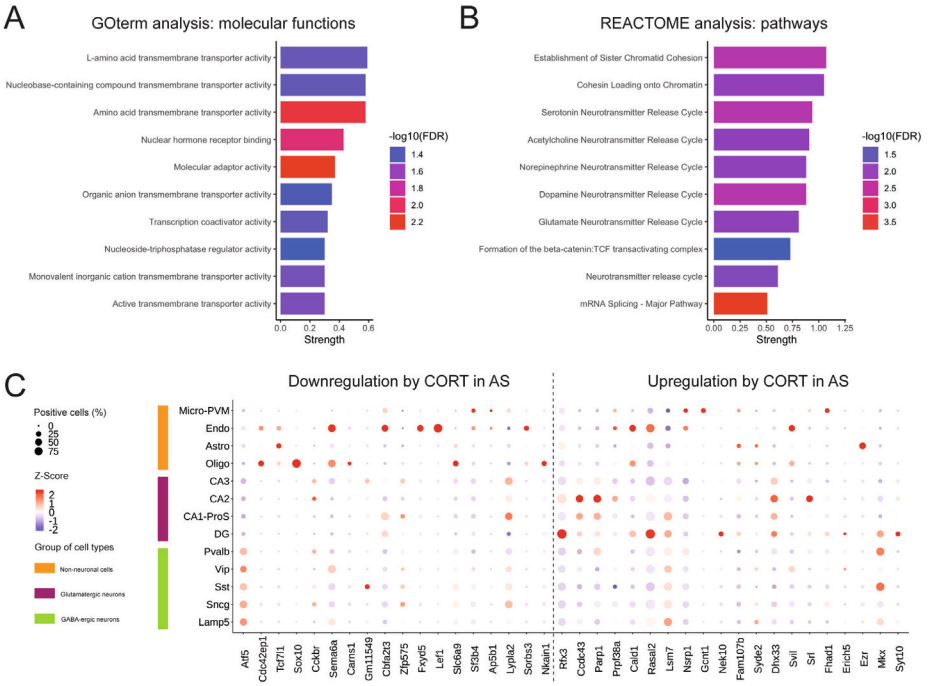

Figure 4. Acute corticosterone exposure in the hippocampus of UBE3A-deficient AS mice influences genes associated with transcription activity and neurotransmitter signaling and are heterogeneously expressed in hippocampal cell types. (A-B) Top 10 terms identified in the (A) gene ontology analysis of molecular functions and (B) REACTOME pathway enrichment analysis associated with the 1,208 genes differentially altered by acute corticosterone treatment in AS mouse hippocampus. The terms were ranked by strength which represents the $\log_{10}$-transformed ratio between the genes annotated with the term to the number of genes expected to be annotated with this term in a random network of comparable size. Enrichment significance is expressed as the - $\log_{10}$(FDR). **(C)** Top 40 genes differentially altered by acute corticosterone treatment in AS mouse hippocampus expression throughout mouse hippocampal cell types. The size of the dots represents the percentage of cells positive for the gene of interest while the colored Z-Score represents the normalized average expression of the gene of interest within one cell type. Cell types were categorized as: non-neuronal cells, glutamatergic neurons, and GABA-ergic neurons. Glutamatergic neurons were separated based on hippocampal sub-regions: the dentate gyrus (DG) and the cornus ammoni regions (CA1-ProS, CA2 and CA3). Genes were divided according to their direction of regulation after acute corticosterone (CORT) treatment in AS.

Continuous CORT exposure does not differentially alter hippocampal GR signaling in UBE3A-deficient AS mice

The detrimental effects of GR disruption in the brain are mostly associated with chronic stress or chronic glucocorticoid exposure. Therefore, we investigated whether continuous CORT treatment of AS mice led to similar or even more pronounced changes in hippocampal GR signaling than the acute treatment. AS and WT mice were implanted subcutaneously with a vehicle pellet or a CORT-releasing pellet, such that CORT was continuously released during five consecutive days (**Fig. 5A**). We again confirmed that UBE3A levels were significantly lower in AS mice brain, as compared to WT ($p < 0.001$), and that continuous CORT treatment did not influence UBE3A protein expression in the frontal cortex (**Fig. 5B, Fig. S2A**).

Two technical outliers were detected (i.e., samples H9 and H13, **Fig. S2B**-**C**) and excluded from the RNA-seq analysis. PCA results showed that 43% of the variation (PC1 + PC2) was attributed to the genotype and treatment effects. Similar to what was observed upon acute CORT treatment, continuous CORT treatment resulted in a clear separation of treated and untreated mice. Vehicle-treated WT and AS mice largely overlapped, and CORT treatment resulted in a modest divergence of WT and AS treated animals (**Fig. 5C**). In response to continuous CORT, the expression of 610 genes was altered in the hippocampus of WT mice (**Fig. 5D**), compared to 773 genes in AS (**Fig. 5E**). Among these CORT-regulated genes, 322 genes overlapped between WT and AS, 288 genes were WT-specific, and 451 genes were AS-specific (**Fig. 5D-E**). The differences between AS and WT in response to continuous CORT exposure were less pronounced than after acute treatment (**Fig 3D-E**). When comparing the CORT treated WT and AS mice, we found only 44 differentially regulated genes, of which none contributed significantly to the genotype-treatment interaction (**Fig. S2D-E**), suggesting that the overall transcriptomic effects of continuous CORT are comparable in WT and AS mouse hippocampus.

Following five days of CORT exposure, we found that the GR levels were slightly, but non significantly, higher in AS brains ($p = 0.058$, **Fig. 5F**). A much larger effect on GR abundance was seen after CORT treatment, which strongly decreased GR protein levels ($p < 0.001$, **Fig. 5F, Fig. S2A**). Altogether, the results indicate that UBE3A deficiency in AS mice does not significantly influence the hippocampal transcriptomic response to continuous CORT exposure.

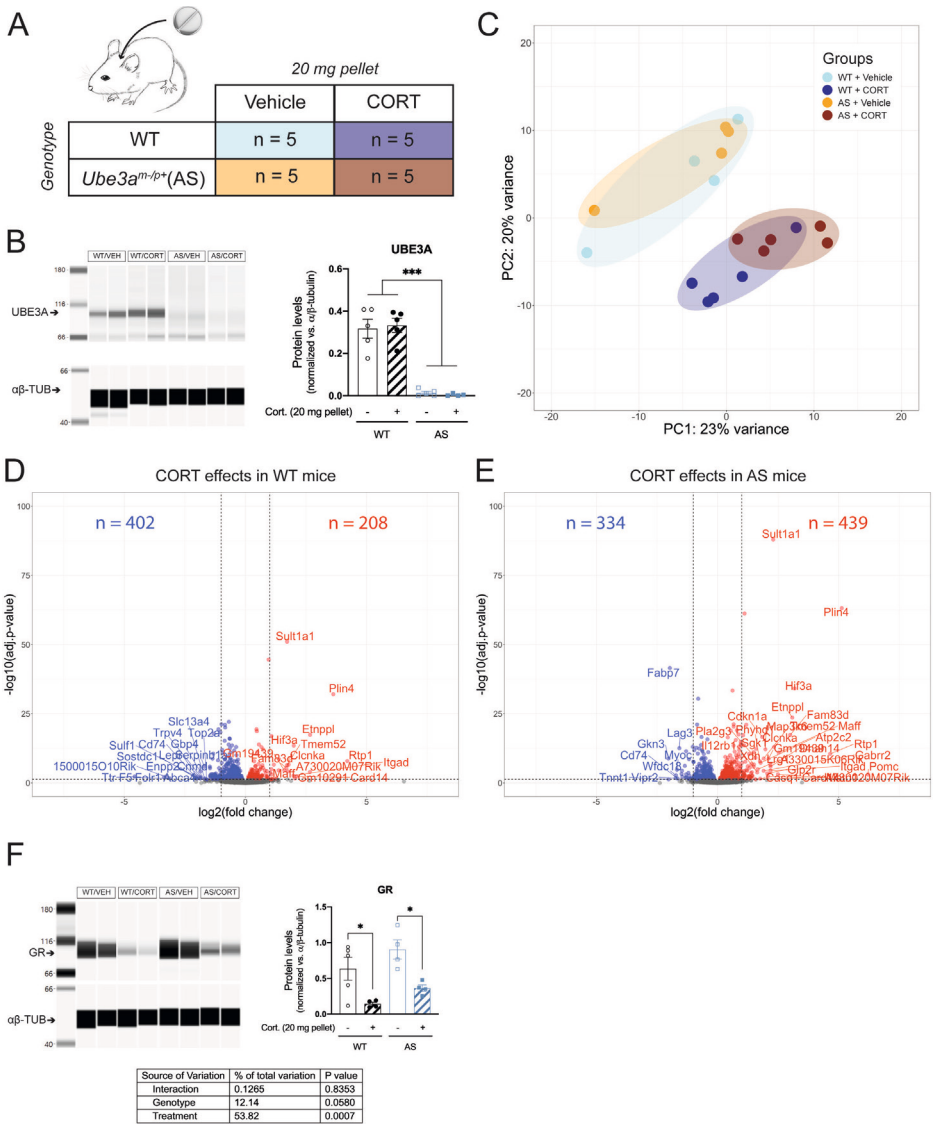

Source of Variation	% of total variation	P value
Interaction	0.1265	0.8353
Genotype	12.14	0.0580
Treatment	53.82	0.0007

Figure 5. Continuous corticosterone exposure does not differentially alter hippocampal GR signaling in UBE3A-deficient AS mice. (A) WT and AS mice were subcutaneously implanted with a vehicle pellet or a slow-release corticosterone (20 mg) pellet for five days (n = 5/group). **(B)** UBE3A protein expression in the frontal cortex of WT and AS mice after continuous treatment with vehicle or corticosterone, normalized against αβ-tubulin levels (αβ-TUB). **(C)** Analysis of hippocampus RNA-seq data principal sources of variance (PCA). **(D)** Volcano plot representing the transcriptomic effects of continuous corticosterone treatment in WT mouse hippocampus. **(E)** Volcano plot representing the transcriptomic effects of continuous corticosterone treatment in AS mouse hippocampus. **(F)** GR protein expression in the frontal cortex of WT and AS mice after continuous treatment with vehicle or corticosterone, normalized against αβ-tubulin levels (αβ-TUB).

Continuous CORT exposure slightly alters liver GR signaling in UBE3A-deficient AS mice

AS mice are known to be susceptible to metabolic disturbances and liver steatosis which can be triggered by chronic glucocorticoid treatment, hence we investigated the peripheral effects of continuous CORT treatment in WT and AS mice using RNA-seq on liver tissue (**Fig. 6A**). As expected, UBE3A was expressed in the AS liver at around 50% of WT levels (due to the active paternal allele in this tissue) (genotype effect: $p < 0.001$, **Fig. 6B**, **Fig. S3A**). According to the PCA results, 48% of the variation (PC1 + PC3) was attributed to the genotype (AS vs. WT) and treatment (CORT vs. vehicle) effects. Comparable to hippocampal data, WT and AS mice showed most overlap upon vehicle treatment and diverged after CORT treatment, which means that most of the effects were driven by CORT treatment (**Fig. 6C**). PC2 corresponded to 23% of the variation and was mostly explained by individual variability between mice (**Fig. S3B-C**).

In total, the expression of 2,484 genes was altered by continuous CORT treatment in the liver of WT mice (**Fig. 6D**), as compared to 3,571 genes in AS mice (**Fig. 6E**). Among these differentially regulated genes, 1,811 genes overlapped between WT and AS, 673 genes were WT-specific, and 1,762 genes were AS-specific (**Fig. 6D-E**). A total of 91 genes were differentially regulated between CORT treated AS and WT mice (**Fig. S3D**), of which only 10 genes statistically contributed to the interaction between the genotype and the treatment (**Fig. S3E**), a dataset too small to perform any adequate GO-term and pathway analyses. In the liver of AS mice, GR protein abundance was significantly higher than in WT mice upon vehicle treatment ($p < 0.05$) and continuous CORT exposure led to a significant decrease in GR levels only in AS mice ($p < 0.01$, **Fig. 6F, Fig. S3A**). Altogether, these results suggest that continuous CORT exposure induces considerable changes in liver transcriptome. Despite the AS-specific decrease in liver GR protein expression upon continuous CORT treatment, only a very small proportion of those transcriptomic effects were specific to AS.

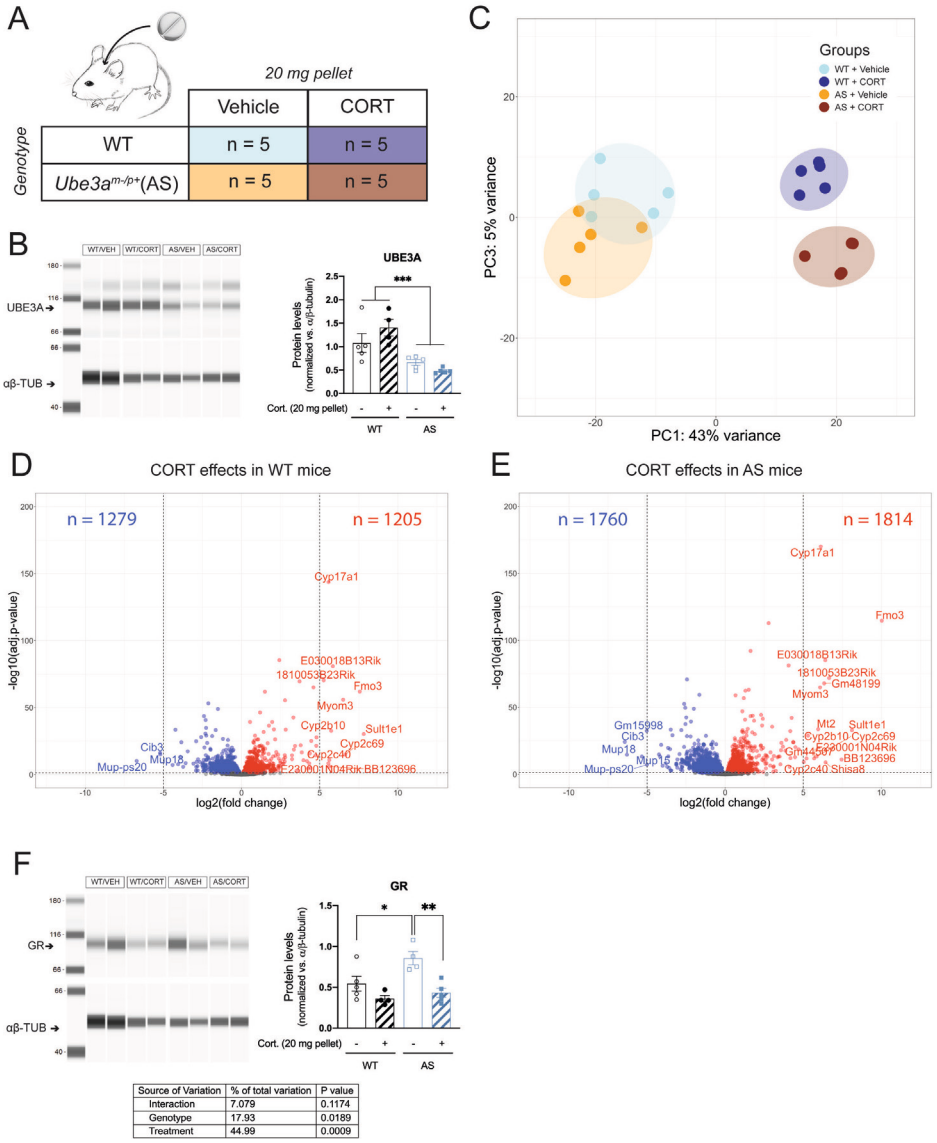

Source of Variation	% of total variation	P value
Interaction	7.079	0.1174
Genotype	17.93	0.0189
Treatment	44.99	0.0009

Figure 6. Continuous corticosterone exposure slightly alters liver GR signaling in UBE3A-deficient AS mice. (A) WT and AS mice were subcutaneously implanted with a vehicle pellet or a slow-release corticosterone (20 mg) pellet for five days (n = 5/group). **(B)** UBE3A protein expression in the liver of WT and AS mice after continuous treatment with vehicle or corticosterone, normalized against αβ-tubulin levels (αβ-TUB). **(C)** Analysis of liver RNA-seq data principal sources of variance (PCA). **(D)** Volcano plot representing the transcriptomic effects of continuous corticosterone treatment in WT mouse liver. **(E)** Volcano plot representing the transcriptomic effects of continuous corticosterone treatment in AS mouse liver. **(F)** GR protein expression in the liver of WT and AS mice after continuous treatment with vehicle or corticosterone, normalized against αβ-tubulin levels (αβ-TUB).

DISCUSSION

UBE3A deficiency in AS has been previously associated with disrupted GR signaling in the hippocampus and impairments in circadian rhythm [33, 35]. In the current study, we confirmed UBE3A interaction with the GR LBD via LxxLL domains and further investigated whether UBE3A-deficient AS mice displayed a differential transcriptomic response to acute and continuous glucocorticoid exposure.

GR transcriptional activity depends on its interactions with coregulator proteins, which bind to either its N-terminal or its C-terminal coregulator binding domain. C-terminal coregulators, associated with the LBD and AF2, possess leucine-rich motifs (LxxLL) which are required to interact with the GR and determine the transcriptional outcome [30, 51]. UBE3A contains three LxxLL motifs [52], two of which showed a significant interaction with the GR LBD. Given the previously reported interaction between full-length UBE3A and GR in mouse brains [33], our results suggest that this binding relies on a physical association between the LBD of GR and these two LxxLL motifs in UBE3A. It is tempting to speculate that the abrogation of this interaction, by mutations in the LxxLL domain, could severely impact the coregulating capability of UBE3A, and contribute to transcriptomic alterations or abnormal behaviors. However, it is difficult to establish how such mutations could specifically affect GR signaling, since UBE3A LxxLL domains have been found to interact with multiple nuclear hormone receptors, including the receptors for estrogen (ERα and ERβ), progesterone (PR), and androgens (AR) [51]. An additional question is whether LxxLL mutations affect the subcellular localization, activity, or stability of UBE3A [16]. If these properties remain largely intact, UBE3A would still be able to function as an E3 ligase for most of its targets, which would prevent LxxLL mutations from causing a typical AS phenotype. These two issues make it difficult to precisely ascertain the pathological contribution of GR dysregulation in AS.

The interaction of UBE3A with GR could precede its ubiquitination and subsequent proteasomal degradation. However, the overexpression of active UBE3A did not significantly decrease GR stability in cells, which indicates that GR is not a typical UBE3A substrate and suggests that the coregulator function of UBE3A may be ligase independent [20, 22]. In line with these results, we found that brain GR levels were not significantly altered in AS mice. However, in AS mice livers, we found GR levels to be significantly higher compared to WT. These results are noteworthy considering that UBE3A expression in peripheral tissue of AS mice is substantially higher than in the brain, and as a consequence, one would expect that the effect on GR levels

would be less pronounced in the liver. This indicates that tissue-specific targeting mechanisms by UBE3A may play a more prominent role in regulating GR levels, rather than UBE3A dosage. Further experiments are necessary to establish whether GR destabilization originates from direct or indirect ligase-dependent effects of UBE3A.

We established that AS mice displayed almost undetectable levels of CORT during the circadian trough, indicating that their HPA axis activity was influenced by UBE3A deficiency. The circadian dynamics of CORT release in the circulation are centrally regulated in the hypothalamic paraventricular nucleus (PVN), which receives negative feedback via the GR [53]. Previous results on circadian rhythmicity in AS mice demonstrated that specifically in neuronal tissue, the lack of UBE3A compromised the turnover of the circadian clock component BMAL1, which led to impaired rhythmicity [35]. Therefore, the lack of UBE3A in PVN neurons could explain the disruption in diurnal CORT release observed in AS mice. Another factor to consider in the context of the alterations in CORT levels is the mineralocorticoid receptor (MR). The MR has a higher affinity to glucocorticoid hormones as compared to the GR [24], and loss of MR function is known to be associated with memory impairments, increased susceptibility to stress, and anxiety-like behaviors [54–56]. However, MR also mediates tonic negative feedback [57], and the differences between AS and WT mice in CORT levels at the circadian trough suggest that MR may be equally or more active in the AS mouse brain.

Our RNA-seq analysis provided genome-wide evidence of an altered hippocampal transcriptome in AS mice following acute CORT exposure. This treatment affected 10 times as many genes in the AS hippocampus as in WT, which suggests that under normal circumstances UBE3A limits GR signaling in the mouse hippocampus. This is in contradiction with our *in vitro* results where GR response to cortisol was decreased in *UBE3A*^{KO} cells, and previous findings in HeLa and Neuro2a cells, where UBE3A acted as a GR transcriptional coactivator [20, 33]. The discrepancy between cell models and our *in vivo* model, warrants further investigation of cell-type specific GR responses, and genomic rather than reporter plasmid readouts to provide more insights into the molecular and cell-type specific events associated with UBE3A-GR interaction.

The majority of the genes that contributed to the acute CORT differences in the AS mouse hippocampus were associated with transcriptional activity; including transcription factors, coactivators, and chromatin remodelers such as *Smarce1*, which was recently associated with an AS-like phenotype in patients with no

molecular diagnostic [58]. Further work is needed to establish how these factors contribute to the differences between AS and WT mice. Besides that, acute CORT treatment in the AS hippocampus also strongly dysregulated genes associated with neurotransmitter signaling. These alterations may disturb synaptic function in CORT-treated AS mice and lead to disruptions in neuronal signaling. Adequate electrophysiological measurements are needed to determine whether CORT exposure leads to measurable alterations in neuronal communication in AS mice. GR is strongly co-expressed with the receptors for serotonin, dopamine, noradrenaline, and acetylcholine in the mouse hippocampal glutamatergic neurons [32], and therefore, disruptions in neurotransmitter signaling could be intertwined with the differential response to CORT in AS mouse hippocampus [59]. There is a multitude of studies that investigated synaptic function in AS mice, collectively reporting cortical and hippocampal neuronal inhibition/excitation imbalances and deficits in hippocampal long-term potentiation [43, 60–63]. Although many synaptic UBE3A substrates have been suggested to effectuate these changes [64–67], the CORT-induced alterations in neurotransmitter genes we report here could similarly underlie the disrupted electrophysiological properties of AS neurons. Dedicated electrophysiological experiments would be needed to determine whether CORT exposure leads to measurable alterations in synaptic function in AS mice.

When mapping the genes that contributed to the differential transcriptomic effects in the hippocampus of AS and WT mice to our scRNA-seq database, we found that their expression was not restricted to neurons. Several corticosterone-responsive genes were also expressed – sometimes exclusively – in astrocytes, oligodendrocytes, endothelial cells, or microglia. In contrast with AS neurons that are devoid of UBE3A protein, non-neuronal AS cells like astrocytes and oligodendrocytes do not undergo epigenetic silencing of the paternal allele of *Ube3a* during maturation and thus still express UBE3A [68]. Our results indicate that, although 50% of UBE3A protein was maintained, acute CORT treatment also affected the transcriptome of non-neuronal AS cells. These findings emphasize that the contribution of non-neuronal cells should be further explored to understand whether the effects in these cells are the result of a decrease in the molecular interaction between UBE3A and GR. Alternatively, the absence of UBE3A in neurons could influence non-neuronal cells via paracrine signaling. In sharp contrast with our findings after acute treatment, no significant genotype-treatment interaction was found in the hippocampus after continuous CORT treatment. This confirms the differences in GR response to acute and continuous CORT treatment in the brain, as expected based on previous findings with acute and chronic stress paradigms [69, 70]. Our results suggest that UBE3A limits the hippocampal acute GR response but not in the context of

prolonged glucocorticoid exposure. However, continuous CORT exposure did lead to a statistical interaction between AS and CORT treatment in the liver transcriptome, which suggests that UBE3A may regulate GR activity in a tissue-specific manner. The observed changes in the liver transcriptomic response to continuous CORT treatment are in line with AS mice susceptibility to hepatic dysfunction [34].

In conclusion, our current study provides novel insight into the molecular interaction between the UBE3A and GR. We demonstrate that AS mice display reduced circulating corticosterone levels during the circadian trough, and a vastly different transcriptomic response in the hippocampus following acute corticosterone treatment. We believe that our findings contribute to a better understanding of the molecular mechanisms of altered glucocorticoid responsiveness in AS. For future research, the corticosterone treatment in AS mice provides a suitable model to investigate the effectiveness of GR antagonists that could compensate for the altered glucocorticoid sensitivity in AS mice, and such treatment strategies could potentially benefit AS patients that suffer from stress and anxiety symptoms [71–75].

REFERENCES

1. Williams CA (2010). The behavioral phenotype of the Angelman syndrome. Am J Med Genet C Semin Med Genet. 154C(4): 432–437. doi: 10.1002/ajmg.c.30278.
2. Buiting K (2010). Prader–Willi syndrome and Angelman syndrome. Am J Med Genet C Semin Med Genet. 154C(3): 365–376. doi: 10.1002/ajmg.c.30273.
3. Buiting K, Williams C, and Horsthemke B (2016). Angelman syndrome — insights into a rare neurogenetic disorder. Nat Rev Neurol. 12(10): 584–593. doi: 10.1038/nrneurol.2016.133.
4. Kishino T, Lalande M, and Wagstaff J (1997). UBE3A/E6-AP mutations cause Angelman syndrome. Nat Genet. 15(1): 70–73. doi: 10.1038/ng0197-70.
5. Matsuura T, Sutcliffe JS, Fang P, Galjaard R-J, Jiang Y, Benton CS, Rommens JM, and Beaudet AL (1997). De novo truncating mutations in E6-AP ubiquitin-protein ligase gene (UBE3A) in Angelman syndrome. Nat Genet. 15(1): 74–77. doi: 10.1038/ng0197-74.
6. Albrecht U, Sutcliffe JS, Cattanach BM, Beechey CV, Armstrong D, Eichele G, and Beaudet AL (1997). Imprinted expression of the murine Angelman syndrome gene, Ube3a, in hippocampal and Purkinje neurons. Nat Genet. 17(1): 75–78. doi: 10.1038/ng0997-75.
7. Sutcliffe JS, Jiang Y, Galjaard R-J, Matsuura T, Fang P, Kubota T, Christian SL, Bressler J, Cattanach B, Ledbetter DH, and Beaudet AL (1997). The E6–AP Ubiquitin–Protein Ligase (UBE3A) Gene Is Localized within a Narrowed Angelman Syndrome Critical Region. Genome Res. 7(4): 368–377. doi: 10.1101/gr.7.4.368.
8. Vu TH, and Hoffman AR (1997). Imprinting of the Angelman syndrome gene, UBE3A, is restricted to brain. Nat Genet. 17(1): 12–13. doi: 10.1038/ng0997-12.
9. Yamasaki K, Joh K, Ohta T, Masuzaki H, Ishimaru T, Mukai T, Niikawa N, Ogawa M, Wagstaff J, and Kishino T (2003). Neurons but not glial cells show reciprocal imprinting of sense and antisense transcripts of Ube3a. Hum Mol Genet. 12(8): 837–847. doi: 10.1093/hmg/ddg106.
10. Lossie AC, Whitney MM, Amidon D, Dong HJ, Chen P, Theriaque D, Hutson A, Nicholls RD, Zori RT, Williams CA, and Driscoll DJ (2001). Distinct phenotypes distinguish the molecular classes of Angelman syndrome. J Med Genet. 38(12): 834–845. doi: 10.1136/jmg.38.12.834.
11. Hershko A, and Ciechanover A (1992). The ubiquitin system for protein degradation. Annu Rev Biochem. 61: 761–807. doi: 10.1146/annurev.bi.61.070192.003553.
12. Huibregtse J m., Scheffner M, and Howley P m. (1991). A cellular protein mediates association of p53 with the E6 oncoprotein of human papillomavirus types 16 or 18. EMBO J. 10(13): 4129–4135. doi: 10.1002/j.1460-2075.1991.tb04990.x.
13. Huibregtse JM, Scheffner M, Beaudenon S, and Howley PM (1995). A family of proteins structurally and functionally related to the E6-AP ubiquitin-protein ligase. Proc Natl Acad Sci. 92(7): 2563–2567. doi: 10.1073/pnas.92.7.2563.
14. Scheffner M, Nuber U, and Huibregtse JM (1995). Protein ubiquitination involving an E1–E2–E3 enzyme ubiquitin thioester cascade. Nature. 373(6509): 81–83. doi: 10.1038/373081a0.
15. Cooper EM, Hudson AW, Amos J, Wagstaff J, and Howley PM (2004). Biochemical Analysis of Angelman Syndrome-associated Mutations in the E3 Ubiquitin Ligase E6-associated Protein*. J Biol Chem. 279(39): 41208–41217. doi: 10.1074/jbc.M401302200.
16. Bossuyt SNV, Punt AM, de Graaf IJ, van den Burg J, Williams MG, Heussler H, Elgersma Y, and Distel B (2021). Loss of nuclear UBE3A activity is the predominant cause of Angelman syndrome in individuals carrying UBE3A missense mutations. Hum Mol Genet. 30(6): 430–442. doi: 10.1093/hmg/ddab050.

17. Avagliano Trezza R, Sonzogni M, Bossuyt SNV, Zampeta FI, Punt AM, van den Berg M, Rotaru DC, Koene LMC, Munshi ST, Stedehouder J, Kros JM, Williams M, Heussler H, de Vrij FMS, Mientjes EJ, van Woerden GM, Kushner SA, Distel B, and Elgersma Y (2019). Loss of nuclear UBE3A causes electrophysiological and behavioral deficits in mice and is associated with Angelman syndrome. Nat Neurosci. 22(8): 1235–1247. doi: 10.1038/s41593-019-0425-0.
18. Yi JJ, Berrios J, Newbern JM, Snider WD, Philpot BD, Hahn KM, and Zylka MJ (2015). An Autism-Linked Mutation Disables Phosphorylation Control of UBE3A. Cell. 162(4): 795–807. doi: 10.1016/j.cell.2015.06.045.
19. Burris TP, Nawaz Z, Tsai MJ, and O'Malley BW (1995). A nuclear hormone receptor-associated protein that inhibits transactivation by the thyroid hormone and retinoic acid receptors. Proc Natl Acad Sci. 92(21): 9525–9529. doi: 10.1073/pnas.92.21.9525.
20. Nawaz Z, Lonard DM, Smith CL, Lev-Lehman E, Tsai SY, Tsai M-J, and O'Malley BW (1999). The Angelman Syndrome-Associated Protein, E6-AP, Is a Coactivator for the Nuclear Hormone Receptor Superfamily. Mol Cell Biol. 19(2): 1182–1189. doi: 10.1128/MCB.19.2.1182.
21. Catoe HW, and Nawaz Z (2011). E6-AP facilitates efficient transcription at estrogen responsive promoters through recruitment of chromatin modifiers. Steroids. 76(9): 897–902. doi: 10.1016/j.steroids.2011.04.007.
22. El Hokayem J, and Nawaz Z (2014). E6AP in the Brain: One Protein, Dual Function, Multiple Diseases. Mol Neurobiol. 49(2): 827–839. doi: 10.1007/s12035-013-8563-y.
23. Joëls M (2018). Corticosteroids and the brain. J Endocrinol. 238(3): R121–R130. doi: 10.1530/JOE-18-0226.
24. de Kloet ER, Joëls M, and Holsboer F (2005). Stress and the brain: from adaptation to disease. Nat Rev Neurosci. 6(6): 463–475. doi: 10.1038/nrn1683.
25. Viho EMG, Buurstede JC, Mahfouz A, Koorneef LL, van Weert LTCM, Houtman R, Hunt HJ, Kroon J, and Meijer OC (2019). Corticosteroid Action in the Brain: The Potential of Selective Receptor Modulation. Neuroendocrinology. 109(3): 266–276. doi: 10.1159/000499659.
26. Goldfarb EV, Rosenberg MD, Seo D, Constable RT, and Sinha R (2020). Hippocampal seed connectome-based modeling predicts the feeling of stress. Nat Commun. 11(1): 2650. doi: 10.1038/s41467-020-16492-2.
27. Spiga F, Walker JJ, Terry JR, and Lightman SL (2014). HPA Axis-Rhythms. In: Compr. Physiol. John Wiley & Sons, Ltd; pp 1273–1298.
28. de Kloet ER, and Sarabdjitsingh RA (2008). Everything Has Rhythm: Focus on Glucocorticoid Pulsatility. Endocrinology. 149(7): 3241–3243. doi: 10.1210/en.2008-0471.
29. Fitzsimons CP, Herbert J, Schouten M, Meijer OC, Lucassen PJ, and Lightman S (2016). Circadian and ultradian glucocorticoid rhythmicity: Implications for the effects of glucocorticoids on neural stem cells and adult hippocampal neurogenesis. Front Neuroendocrinol. 41: 44–58. doi: 10.1016/j.yfrne.2016.05.001.
30. Weikum ER, Knuesel MT, Ortlund EA, and Yamamoto KR (2017). Glucocorticoid receptor control of transcription: precision and plasticity via allostery. Nat Rev Mol Cell Biol. 18(3): 159–174. doi: 10.1038/nrm.2016.152.
31. Mahfouz A, Lelieveldt BPF, Grefhorst A, van Weert LTCM, Mol IM, Sips HCM, van den Heuvel JK, Datson NA, Visser JA, Reinders MJT, and Meijer OC (2016). Genome-wide coexpression of steroid receptors in the mouse brain: Identifying signaling pathways and functionally coordinated regions. Proc Natl Acad Sci. 113(10): 2738–2743. doi: 10.1073/pnas.1520376113.
32. Viho EMG, Buurstede JC, Berkhout JB, Mahfouz A, and Meijer OC (2022). Cell type specificity of glucocorticoid signaling in the adult mouse hippocampus. J Neuroendocrinol. 34(2): e13072. doi: 10.1111/jne.13072.

33. Godavarthi SK, Dey P, Maheshwari M, and Ranjan Jana N (2012). Defective glucocorticoid hormone receptor signaling leads to increased stress and anxiety in a mouse model of Angelman syndrome. Hum Mol Genet. 21(8): 1824–1834. doi: 10.1093/hmg/ddr614.
34. Kim J, Lee B, Kim D-H, Yeon JG, Lee J, Park Y, Lee Y, Lee S-K, Lee S, and Lee JW (2019). UBE3A Suppresses Overnutrition-Induced Expression of the Steatosis Target Genes of MLL4 by Degrading MLL4. Hepatology. 69(3): 1122–1134. doi: https://doi.org/10.1002/hep.30284.
35. Shi S, Bichell TJ, Ihrie RA, and Johnson CH (2015). Ube3a Imprinting Impairs Circadian Robustness in Angelman Syndrome Models. Curr Biol. 25(5): 537–545. doi: 10.1016/j.cub.2014.12.047.
36. Koorneef LL, van den Heuvel JK, Kroon J, Boon MR, 't Hoen PAC, Hettne KM, van de Velde NM, Kolenbrander KB, Streefland TCM, Mol IM, Sips HCM, Kielbasa SM, Mei H, Belanoff JK, Pereira AM, Oosterveer MH, Hunt H, Rensen PCN, and Meijer OC (2018). Selective Glucocorticoid Receptor Modulation Prevents and Reverses Nonalcoholic Fatty Liver Disease in Male Mice. Endocrinology. 159(12): 3925–3936. doi: 10.1210/en.2018-00671.
37. Kroon J, Schilperoort M, In het Panhuis W, van den Berg R, van Doeselaar L, Verzijl CRC, van Trigt N, Mol IM, Sips HHCM, van den Heuvel JK, Koorneef LL, van der Sluis RJ, Fenzl A, Kiefer FW, Vettorazzi S, Tuckermann JP, Biermasz NR, Meijer OC, Rensen PCN, and Kooijman S (2021). A physiological glucocorticoid rhythm is an important regulator of brown adipose tissue function. Mol Metab. 47: 101179. doi: 10.1016/j.molmet.2021.101179.
38. Rahimi L, Rajpal A, and Ismail-Beigi F (2020). Glucocorticoid-Induced Fatty Liver Disease. Diabetes Metab Syndr Obes Targets Ther. 13: 1133–1145. doi: 10.2147/DMSO.S247379.
39. Desmet SJ, Dejager L, Clarisse D, Thommis J, Melchers D, Bastiaensen N, Ruijtenbeek R, Beck IM, Libert C, Houtman R, Meijer OC, and De Bosscher K (2014). Cofactor Profiling of the Glucocorticoid Receptor from a Cellular Environment. In: Castoria G, Auricchio F, editors Steroid Recept. Methods Protoc. Springer, New York, NY; pp 83–94.
40. Zampeta FI, Sonzogni M, Niggl E, Lendemeijer B, Smeenk H, de Vrij FMS, Kushner SA, Distel B, and Elgersma Y (2020). Conserved UBE3A subcellular distribution between human and mice is facilitated by non-homologous isoforms. Hum Mol Genet. 29(18): 3032–3043. doi: 10.1093/hmg/ddaa194.
41. Morales J et al. (2022). A joint NCBI and EMBL-EBI transcript set for clinical genomics and research. Nature. 604(7905): 310–315. doi: 10.1038/s41586-022-04558-8.
42. Liu W, Wang J, Yu G, and Pearce D (1996). Steroid receptor transcriptional synergy is potentiated by disruption of the DNA-binding domain dimer interface. Mol Endocrinol. 10(11): 1399–1406. doi: 10.1210/mend.10.11.8923466.
43. Jiang Y, Armstrong D, Albrecht U, Atkins CM, Noebels JL, Eichele G, Sweatt JD, and Beaudet AL (1998). Mutation of the Angelman Ubiquitin Ligase in Mice Causes Increased Cytoplasmic p53 and Deficits of Contextual Learning and Long-Term Potentiation. Neuron. 21(4): 799–811. doi: 10.1016/S0896-6273(00)80596-6.
44. Buurstede JC, Umeoka EHL, da Silva MS, Krugers HJ, Joëls M, and Meijer OC (2022). Application of a pharmacological transcriptome filter identifies a shortlist of mouse glucocorticoid receptor target genes associated with memory consolidation. Neuropharmacology. 216: 109186. doi: 10.1016/j.neuropharm.2022.109186.
45. Buurstede JC, van Weert LTCM, Colucci P, Gentenaar M, Viho EMG, Koorneef LL, Schoonderwoerd RA, Lanooij SD, Moustakas I, Balog J, Mei H, Kielbasa SM, Campolongo P, Roozendaal B, and Meijer OC (2022). Hippocampal glucocorticoid target genes associated with enhancement of memory consolidation. Eur J Neurosci. 55(9–10): 2666–2683. doi: 10.1111/ejn.15226.

46. Atucha E, Zalachoras I, van den Heuvel JK, van Weert LTCM, Melchers D, Mol IM, Belanoff JK, Houtman R, Hunt H, Roozendaal B, and Meijer OC (2015). A Mixed Glucocorticoid/Mineralocorticoid Selective Modulator With Dominant Antagonism in the Male Rat Brain. Endocrinology. 156(11): 4105–4114. doi: 10.1210/en.2015-1390.
47. Spaanderman DCE, Nixon M, Buurstede JC, Sips HHCM, Schilperoort M, Kuipers EN, Backer EA, Kooijman S, Rensen PCN, Homer NZM, Walker BR, Meijer OC, and Kroon J (2019). Androgens modulate glucocorticoid receptor activity in adipose tissue and liver. J Endocrinol. 240(1): 51–63. doi: 10.1530/JOE-18-0503.
48. Viho EM, Kroon J, Feelders RA, Houtman R, Dungen E van den, Arias AMP, Hunt H, Hofland LJ, and Meijer OC (2022). Peripheral glucocorticoid receptor antagonism by relacorilant with modest HPA axis disinhibition. J Endocrinol. 1(aop). doi: 10.1530/JOE-22-0263.
49. Koorneef LL, Kroon J, Viho EMG, Wahl LF, Heckmans KML, Dorst MMAR van, Hoekstra M, Houtman R, Hunt H, and Meijer OC (2020). The selective glucocorticoid receptor antagonist CORT125281 has tissue-specific activity. J Endocrinol. 246(1): 79–92. doi: 10.1530/JOE-19-0486.
50. Szklarczyk D, Gable AL, Lyon D, Junge A, Wyder S, Huerta-Cepas J, Simonovic M, Doncheva NT, Morris JH, Bork P, Jensen LJ, and Mering C von (2019). STRING v11: protein–protein association networks with increased coverage, supporting functional discovery in genome-wide experimental datasets. Nucleic Acids Res. 47(D1): D607–D613. doi: 10.1093/nar/gky1131.
51. Broekema MF, Hollman DAA, Koppen A, van den Ham H-J, Melchers D, Pijnenburg D, Ruijtenbeek R, van Mil SWC, Houtman R, and Kalkhoven E (2018). Profiling of 3696 Nuclear Receptor–Coregulator Interactions: A Resource for Biological and Clinical Discovery. Endocrinology. 159(6): 2397–2407. doi: 10.1210/en.2018-00149.
52. Ramamoorthy S, and Nawaz Z (2008). E6-associated protein (E6-AP) is a dual function coactivator of steroid hormone receptors. Nucl Recept Signal. 6(1): nrs.06006. doi: 10.1621/nrs.06006.
53. Spencer RL, and Deak T (2017). A users guide to HPA axis research. Physiol Behav. 178: 43–65. doi: 10.1016/j.physbeh.2016.11.014.
54. Berger S, Wolfer DP, Selbach O, Alter H, Erdmann G, Reichardt HM, Chepkova AN, Welzl H, Haas HL, Lipp H-P, and Schütz G (2006). Loss of the limbic mineralocorticoid receptor impairs behavioral plasticity. Proc Natl Acad Sci. 103(1): 195–200. doi: 10.1073/pnas.0503878102.
55. ter Heegde F, De Rijk RH, and Vinkers CH (2015). The brain mineralocorticoid receptor and stress resilience. Psychoneuroendocrinology. 52: 92–110. doi: 10.1016/j.psyneuen.2014.10.022.
56. Lightman SL, Birnie MT, and Conway-Campbell BL (2020). Dynamics of ACTH and Cortisol Secretion and Implications for Disease. Endocr Rev. 41(3): bnaa002. doi: 10.1210/endrev/bnaa002.
57. Ratka A, Sutanto W, Bloemers M, and Kloet R de (1989). On the Role of Brain Mineralocorticoid (Type I) and Glucocorticoid (Type II) Receptors in Neuroendocrine Regulation. Neuroendocrinology. 50(2): 117–123. doi: 10.1159/000125210.
58. Aguilera C, Gabau E, Ramirez-Mallafré A, Brun-Gasca C, Dominguez-Carral J, Delgadillo V, Laurie S, Derdak S, Padilla N, Cruz X de la, Capdevila N, Spataro N, Baena N, Guitart M, and Ruiz A (2021). New genes involved in Angelman syndrome-like: Expanding the genetic spectrum. PLOS ONE. 16(10): e0258766. doi: 10.1371/journal.pone.0258766.
59. Farook MF, DeCuypere M, Hyland K, Takumi T, LeDoux MS, and Reiter LT (2012). Altered Serotonin, Dopamine and Norepinepherine Levels in 15q Duplication and Angelman Syndrome Mouse Models. PLOS ONE. 7(8): e43030. doi: 10.1371/journal.pone.0043030.

60. Kaphzan H, Buffington SA, Jung JI, Rasband MN, and Klann E (2011). Alterations in intrinsic membrane properties and the axon initial segment in a mouse model of Angelman syndrome. J Neurosci Off J Soc Neurosci. 31(48): 17637–17648. doi: 10.1523/JNEUROSCI.4162-11.2011.
61. Rotaru DC, Woerden GM van, Wallaard I, and Elgersma Y (2018). Adult Ube3a Gene Reinstatement Restores the Electrophysiological Deficits of Prefrontal Cortex Layer 5 Neurons in a Mouse Model of Angelman Syndrome. J Neurosci. 38(37): 8011–8030. doi: 10.1523/JNEUROSCI.0083-18.2018.
62. Silva-Santos S, Woerden GM van, Bruinsma CF, Mientjes E, Jolfaei MA, Distel B, Kushner SA, and Elgersma Y (2015). *Ube3a* reinstatement identifies distinct developmental windows in a murine Angelman syndrome model. J Clin Invest. 125(5): 2069–2076. doi: 10.1172/JCI80554.
63. Judson MC, Wallace ML, Sidorov MS, Burette AC, Gu B, van Woerden GM, King IF, Han JE, Zylka MJ, Elgersma Y, Weinberg RJ, and Philpot BD (2016). GABAergic Neuron-Specific Loss of Ube3a Causes Angelman Syndrome-Like EEG Abnormalities and Enhances Seizure Susceptibility. Neuron. 90(1): 56–69. doi: 10.1016/j.neuron.2016.02.040.
64. Sun J, Zhu G, Liu Y, Standley S, Ji A, Tunuguntla R, Wang Y, Claus C, Luo Y, Baudry M, and Bi X (2015). UBE3A Regulates Synaptic Plasticity and Learning and Memory by Controlling SK2 Channel Endocytosis. Cell Rep. 12(3): 449–461. doi: 10.1016/j.celrep.2015.06.023.
65. Egawa K, Kitagawa K, Inoue K, Takayama M, Takayama C, Saitoh S, Kishino T, Kitagawa M, and Fukuda A (2012). Decreased Tonic Inhibition in Cerebellar Granule Cells Causes Motor Dysfunction in a Mouse Model of Angelman Syndrome. Sci Transl Med. 4(163): 163ra157-163ra157. doi: 10.1126/scitranslmed.3004655.
66. Margolis SS, Salogiannis J, Lipton DM, Mandel-Brehm C, Wills ZP, Mardinly AR, Hu L, Greer PL, Bikoff JB, Ho H-YH, Soskis MJ, Sahin M, and Greenberg ME (2010). EphB-Mediated Degradation of the RhoA GEF Ephexin5 Relieves a Developmental Brake on Excitatory Synapse Formation. Cell. 143(3): 442–455. doi: 10.1016/j.cell.2010.09.038.
67. Kaphzan H, Buffington SA, Ramaraj AB, Lingrel JB, Rasband MN, Santini E, and Klann E (2013). Genetic Reduction of the α1 Subunit of Na/K-ATPase Corrects Multiple Hippocampal Phenotypes in Angelman Syndrome. Cell Rep. 4(3): 405–412. doi: 10.1016/j.celrep.2013.07.005.
68. Judson MC, Sosa-Pagan JO, Del Cid WA, Han JE, and Philpot BD (2014). Allelic specificity of Ube3a Expression In The Mouse Brain During Postnatal Development. J Comp Neurol. 522(8): 1874–1896. doi: 10.1002/cne.23507.
69. Flati T, Gioiosa S, Chillemi G, Mele A, Oliverio A, Mannironi C, Rinaldi A, and Castrignanò T (2020). A gene expression atlas for different kinds of stress in the mouse brain. Sci Data. 7(1): 437. doi: 10.1038/s41597-020-00772-z.
70. Filipović D, Zlatković J, Gass P, and Inta D (2013). The differential effects of acute vs. chronic stress and their combination on hippocampal parvalbumin and inducible heat shock protein 70 expression. Neuroscience. 236: 47–54. doi: 10.1016/j.neuroscience.2013.01.033.
71. Wheeler AC, Sacco P, and Cabo R (2017). Unmet clinical needs and burden in Angelman syndrome: a review of the literature. Orphanet J Rare Dis. 12(1): 164. doi: 10.1186/s13023-017-0716-z.
72. Wheeler AC, Okoniewski KC, Wylie A, DeRamus M, Hiruma LS, Toth D, and Christian RB (2019). Anxiety-associated and separation distress-associated behaviours in Angelman syndrome. J Intellect Disabil Res. 63(10): 1234–1247. doi: 10.1111/jir.12635.
73. Gentile JK, Tan W-H, Horowitz LT, Bacino CA, Skinner SA, Barbieri-Welge R, Bauer-Carlin A, Beaudet AL, Bichell TJ, Lee H-S, Sahoo T, Waisbren SE, Bird LM, and Peters SU (2010). A Neurodevelopmental Survey of Angelman Syndrome With Genotype-Phenotype Correlations. J Dev Behav Pediatr. 31(7): 592–601. doi: 10.1097/DBP.0b013e3181ee408e.

74. Wink LK, Fitzpatrick S, Shaffer R, Melnyk S, Begtrup AH, Fox E, Schaefer TL, Mathieu-Frasier L, Ray B, Lahiri D, Horn PA, and Erickson CA (2015). The neurobehavioral and molecular phenotype of Angelman Syndrome. Am J Med Genet A. 167(11): 2623–2628. doi: 10.1002/ajmg.a.37254.
75. Keary CJ, Mullett JE, Nowinski L, Wagner K, Walsh B, Saro HK, Erhabor G, Thibert RL, McDougle CJ, and Ravichandran CT (2022). Parent Description of Anxiety in Angelman Syndrome. J Autism Dev Disord. 52(8): 3612–3625. doi: 10.1007/s10803-021-05238-8.

ACKNOWLEDGEMENTS

The authors would like to thank Ilse Wallaard and Hetty Sips for their technical support with the animal experiments and the protein assays, respectively. We thank Jacobus C. Buurstede and Leon Mei for their expertise and their contribution to the RNA sequencing analyses, and Lotte Rietman for her contribution to gene ontology analysis. Finally, we thank Karolien De Bosscher who generously provided the human GR plasmid.

APPENDIX

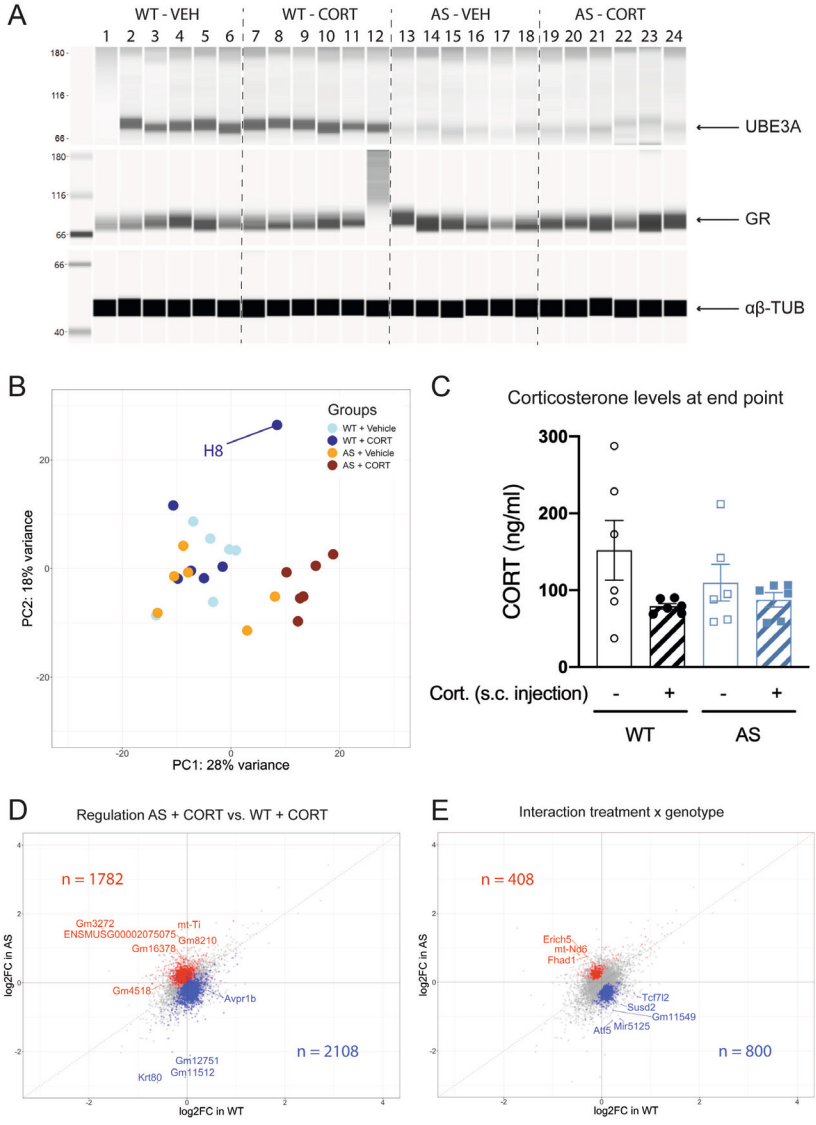

Figure S1. Consequences of acute corticosterone exposure in the AS mouse brain. (A) Protein expression of UBE3A, GR and αβ-tubulin (αβ-TUB) in WT and AS mouse brain after acute treatment with vehicle or 3mg/kg corticosterone. **(B)** Sample H8 explains 18% of the RNA-seq variance. **(C)** Endpoint corticosterone plasma levels (ng/mL) measured from mouse trunk blood. **(D)** Fold change-fold change plot summarizing the contrast between AS and WT mice treated with acute corticosterone. **(E)** Fold change-fold change plot displaying the genes that significantly contributed to the differential response to acute corticosterone in AS mouse hippocampus.

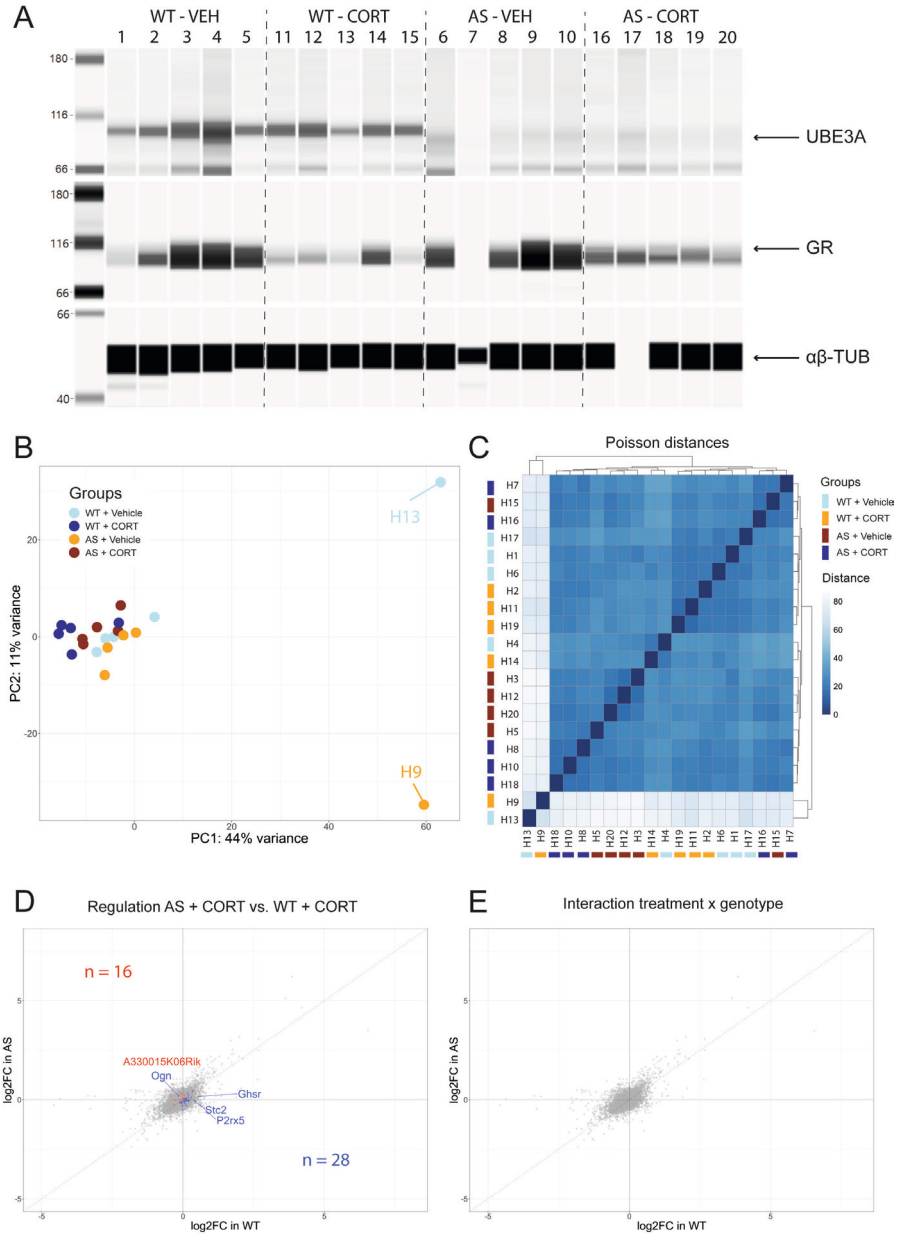

Figure S2. Consequences of continuous corticosterone exposure in the AS mouse brain. **(A)** Protein expression of UBE3A, GR and αβ-tubulin (αβ-TUB) in WT and AS mouse brain after continuous treatment with vehicle or corticosterone (20 mg releasing-pellet). **(B)** Samples H9 and H13 biased the variance analysis. **(C)** Samples H9 and H13 were technical outliers as determined by the Poisson distance analysis. **(D)** Fold change-fold change plot summarizing the contrast between AS and WT mice treated with continuous corticosterone. **(E)** Fold change-fold change plot displaying the genes that significantly contributed to the differential response to continuous corticosterone in AS mouse hippocampus.

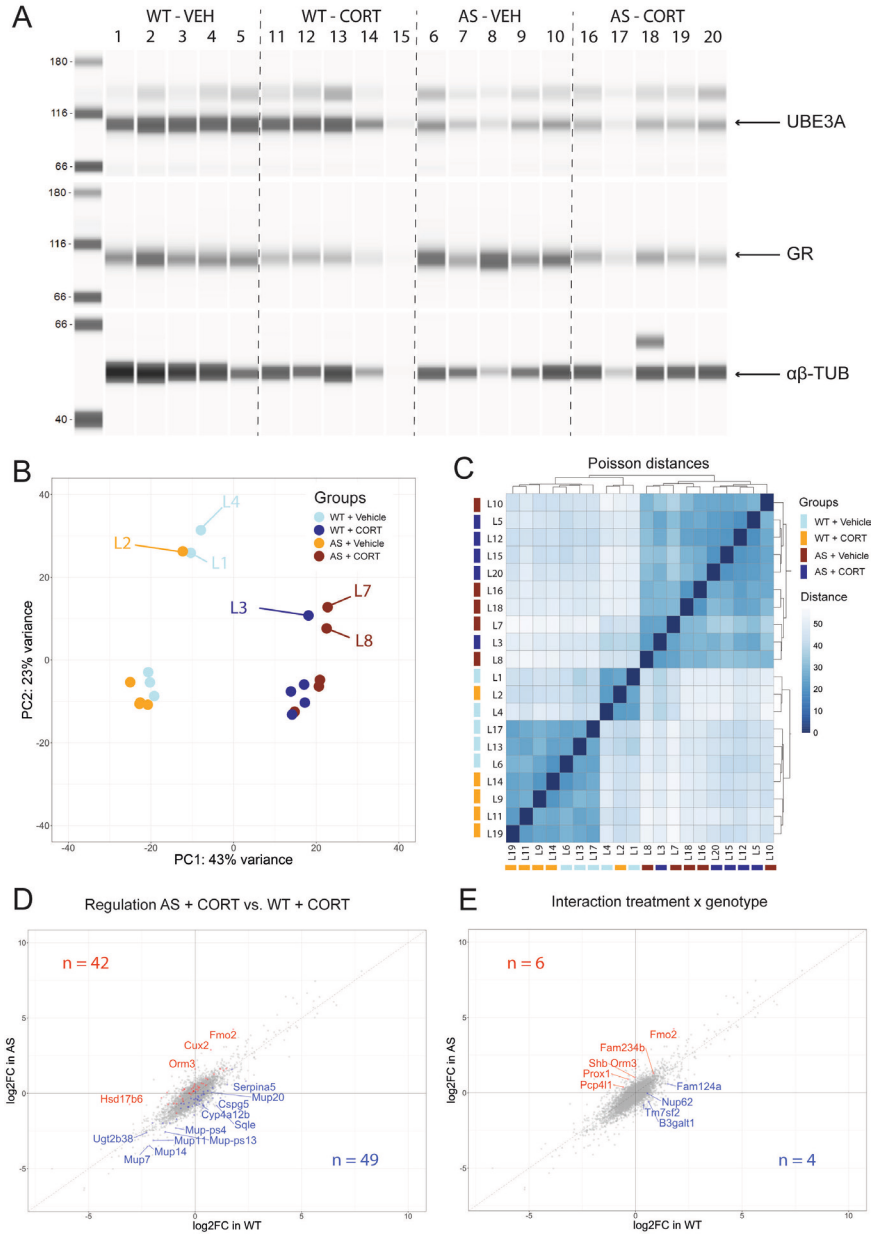

Figure S3. Consequences of continuous corticosterone exposure in the AS mouse liver. **(A)** Protein expression of UBE3A, GR and αβ-tubulin (αβ-TUB) in WT and AS mouse liver after continuous treatment with vehicle or corticosterone (20 mg releasing-pellet). **(B)** Biological variability between mice contributed to 23% of the RNA-seq variance. **(C)** The Poisson distance analysis did not highlight specific outliers. **(D)** Fold change-fold change plot summarizing the contrast between AS and WT mice treated with continuous corticosterone. **(E)** Fold change-fold change plot displaying the genes that significantly contributed to the differential response to continuous corticosterone in AS mouse liver.

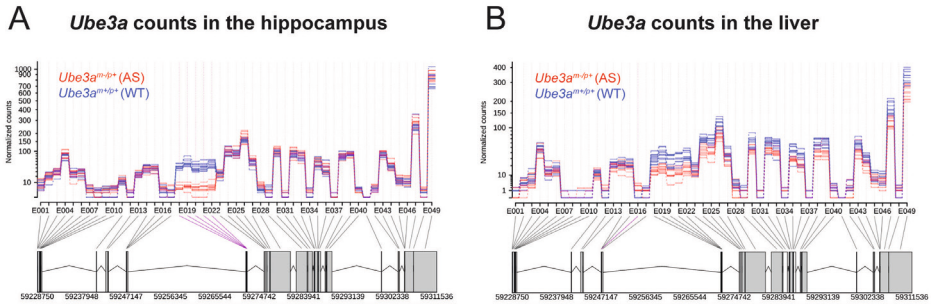

Figure S4. Differential exon usage analysis of *Ube3a*. (A) Exon usage plot of *Ube3a* in the AS mouse hippocampus, **(B)** and liver.